

# Fractal dimension of the cosmic web with different galaxy types

Ana Elisa Lima<sup>a,1</sup>, Julianne C. Soares<sup>b,2</sup>, Ana Carolina S. Tavares<sup>c,3</sup>, Mariana V. Taveira<sup>d,4</sup>, Sharon Teles<sup>e,f,5</sup>, Amanda R. Lopes<sup>g,h,6</sup>, Marcelo B. Ribeiro<sup>e,f,7,\*</sup>

<sup>a</sup>*Chemistry Institute, Universidade Estadual de Campinas, Campinas, Brazil*

<sup>b</sup>*Geosciences Institute, Universidade Federal do Rio de Janeiro, Rio de Janeiro, Brazil*

<sup>c</sup>*Faculty of Animal Science and Food Engineering, Universidade de São Paulo, São Paulo, Brazil*

<sup>d</sup>*Division of Physics, Mathematics and Astronomy, California Institute of Technology, USA*

<sup>e</sup>*Physics Institute, Universidade Federal do Rio de Janeiro, Rio de Janeiro, Brazil*

<sup>f</sup>*Graduate Program in Applied Physics–PPGMFA, Universidade Federal do Rio de Janeiro, Brazil*

<sup>g</sup>*Instituto de Astrofísica de La Plata, CONICET-UNLP, La Plata, Argentina*

<sup>h</sup>*Institute of Astronomy, Geophysics, and Atmospheric Sciences, Universidade de São Paulo, São Paulo, Brazil*

---

## Abstract

The fractal dimension  $D$  is used to map the large-scale galaxy distribution in the Universe by color types: blue, green and red. Using a  $NUVrK$ -complete COSMOS2020 subsample of 618,952 galaxies observed up to  $z = 4$ , number densities were derived and plotted against two cosmological distance measures, the luminosity and comoving (galaxy area) distances, in order to estimate  $D$  for each galaxy color type in two redshift intervals:  $z \gtrless 1$ . We found a general gradient  $D_{\text{blue}} > D_{\text{red}} > D_{\text{green}}$  with  $D = 1.40 - 2.03$  for  $z < 1$ . For  $1 < z \leq 4$ , the gradient changes to  $D_{\text{blue}} > D_{\text{green}} > D_{\text{red}}$ , and the fractal dimension values are lower,  $D = 0.03 - 0.44$ . These results suggest that the fractal dimension is a sensitive diagnostic for how galaxy populations trace the evolving cosmic web, and confirm the fractal dimension as a useful tool for observational mapping of large-scale structure by galaxy color.

*Keywords:* cosmology, large-scale structure of the universe, fractals, galaxy distribution, galaxy color types

---

\*Corresponding author

Email addresses: [a204409@dac.unicamp.br](mailto:a204409@dac.unicamp.br) (Ana Elisa Lima), [julianne@ufrj.br](mailto:julianne@ufrj.br) (Julianne C. Soares), [tavares.carolina@usp.br](mailto:tavares.carolina@usp.br) (Ana Carolina S. Tavares), [mtaveira@caltech.edu](mailto:mtaveira@caltech.edu) (Mariana V. Taveira), [steles.ts@gmail.com](mailto:steles.ts@gmail.com) (Sharon Teles), [amandalopes1920@gmail.com](mailto:amandalopes1920@gmail.com) (Amanda R. Lopes), [mbr@if.ufrj.br](mailto:mbr@if.ufrj.br) (Marcelo B. Ribeiro)

<sup>1</sup>Orcid 0009-0007-9041-9014

<sup>2</sup>Orcid 0009-0005-6305-4860

<sup>3</sup>Orcid 0009-0002-8403-6299

<sup>4</sup>Orcid 0009-0002-8012-390X

<sup>5</sup>Orcid 0000-0003-4497-9161

<sup>6</sup>Orcid 0000-0002-6164-5051

<sup>7</sup>Orcid 0000-0002-6919-2624

## 1. Introduction

Galaxies are distributed in a highly clustered and void-dominated fashion, an irregular pattern that makes fractal geometry attractive for describing large scale topology and, possibly, galaxy evolution. Galaxies have various shapes, sizes, and colors, then to try to understand how their morphologies are related to their physical features requires classification in some way [1]. However, the breadth of galaxy properties makes galaxy classification challenging.

Advances in observational technology in recent decades have supplied researchers with galaxy redshift surveys reaching distances previously inaccessible. Large surveys have mapped the Universe with increasing details, revealing a structurally rich cosmos and providing critical data for testing cosmological models. One of these tests is if the galaxy distribution inhomogeneous pattern would become homogeneous at larger scales, a subject where fractal geometry can be useful as it provides ways of characterizing very irregular structures [2]. This is so because the single fractal dimension  $D$  measures the degree of inhomogeneity since the irregularly distributed galaxy system is viewed as self-similar, and, therefore, forming a fractal system in which  $D$  quantitatively depicts galactic clustering sparsity or, complementarily, the dominance of voids in the large-scale structure of the Universe [3–5], even connecting with galaxy mergers [6]. Fractals have so far been mainly used in cosmology to discuss this problem, with arguments pro [7–12] and against [13, 14] an unlimited galaxy fractal system up to our present observations, and possibly beyond, although a theoretical prediction that the standard cosmological model does allow for unlimited *observational* inhomogeneity was advanced some decades ago [15–20].

The aim of this work is to use fractal geometry for galaxy clustering classification. So, here we shall not focus on the problem of if observations indicate an unlimited, irregularly distributed, fractal galaxy system. The starting point of this study was a by-product of Ref. [11] showing that galaxies with different colors exhibit different single fractal dimensions at different redshift ranges once their distribution is constructed using cumulative number counts vis-à-vis various relativistic cosmological distances. This by-product revealed that in the COSMOS2015 survey red galaxies have single fractal dimensions  $D$  bigger than blue galaxies for  $z < 1$ , whereas the situation is the opposite for  $z > 1$ . For the SPLASH survey blue galaxies have  $D$  bigger than red galaxies [11]. So, the aim here is to further analyze this feature with a much bigger and up-to-date galaxy survey in order to confirm the fractal dimension as a sensitive diagnostic for how galaxy population types trace the evolving large-scale clustering.

The data used here are formed by a subsample of the COSMOS2020 [21] galaxy catalog. The filtering process was based on photometric characteristics, selecting galaxies having  $z \leq 6$  and magnitudes in the near-ultraviolet, optical, and near-infrared: NUV, r, and K bands. The goal was to categorize galaxies into three color types: blue, green and red. The results showed clear dependence of the fractal dimension with galaxy colors:  $D_{\text{blue}} > D_{\text{red}} > D_{\text{green}}$  having fractal dimension varying in the range  $D = 1.40 - 2.03$  for  $z < 1$ , and  $D_{\text{blue}} > D_{\text{green}} > D_{\text{red}}$  in the range  $D = 0.03 - 0.44$  for  $1 < z \leq 4$ .

This paper is structured as follows. Sec. 2 presents the fractal analysis methodology

concerning the use of relativistic distances for the attainment of the numerical densities of galaxies. Sec. 3 describes the COSMOS2020 survey and the data characteristics relevant to this work. Sec. 4 describes the sample selection criteria, including a tool for classifying galaxies by color using the fractal dimension. Sec. 5 presents the results and Sec. 6 is constituted by our conclusions.

## 2. Fractal galaxy distribution

The theoretical basis of the fractal method capable of characterizing how galaxies are irregularly distributed in space is conceptually very simple and straightforward to apply. It is based on a fundamental hypothesis for the empirical description of galaxy distribution called the *Pietronero-Wertz number distance relation*, which can be written as follows,

$$N_{\text{obs}} = B (d_{\text{obs}})^D. \quad (1)$$

Here  $N_{\text{obs}}$  is the *observed cumulative number counts* of galaxies,  $B$  is a positive constant,  $d_{\text{obs}}$  is an *observational distance*, and  $D$  is the single fractal dimension. Eq. (1) was first advanced by Wertz [22, 23] under a different terminology. Later it was independently rederived and interpreted under a fractal framework by Pietronero [3; see also 5, §III.4, and 24, §3]. As we shall show below this expression can be very easily connected to other observational quantities [see also 11, and 12, §1.2, app. B].

Let  $V_{\text{obs}}$  be the *observational volume* and  $\gamma_{\text{obs}}^*$  the *observed number density*, respectively written as follows,

$$V_{\text{obs}} = \frac{4}{3}\pi(d_{\text{obs}})^3, \quad (2)$$

$$\gamma_{\text{obs}}^* = \frac{N_{\text{obs}}}{V_{\text{obs}}}. \quad (3)$$

Now, substituting Eqs. (1) and (2) into Eq. (3) we obtain the *de Vaucouleurs density power-law* [25],

$$\gamma_{\text{obs}}^* = \frac{3B}{4\pi}(d_{\text{obs}})^{D-3}. \quad (4)$$

The interplay among these quantities falls in two possible situations. If  $D = 3$  both  $N_{\text{obs}}$  and  $V_{\text{obs}}$  grow at the same pace with increasing values of  $d_{\text{obs}}$ , which then means that galaxies are evenly distributed along the observed space as  $\gamma_{\text{obs}}^*$  remains constant. If  $D < 3$  then  $N_{\text{obs}}$  grows at a smaller rate than  $V_{\text{obs}}$ , which then creates gaps, or voids, in the galactic distribution as well as regions where galaxies clump. This is so because the fractal dimension of these structures depend on how  $N_{\text{obs}}$  grows cumulatively: its rate of increase could vary with  $d_{\text{obs}}$ , which then affects the value of  $D$  and cause  $\gamma_{\text{obs}}^*$  to vary. Hence, voids and galaxy clusters are a by-product of the galaxy fractal system when  $D$  is smaller than the topological dimension where the galaxy structure is embedded. Eq. (4) provides the empirical method for detecting such a variation between  $N_{\text{obs}}$  and  $d_{\text{obs}}$  by measuring the power-law slope in a log-log plot which in turn determines  $D$ .

Eqs. (1) to (4) are straightforwardly applied to the Newtonian cosmology approximation, but this is only possible up to  $z \approx 0.2$  because beyond this range the various distance measures differ for the same redshift value due to relativistic effects [16, 18–20]. Previous works dealing with observations under a fractal cosmology scenario have used various cosmological distance definitions [9, 11, 12], but here it suffices to restrict ourselves only to the *luminosity distance*  $d_L$  and *galaxy area distance*  $d_G$ , also known as *transverse comoving distance* [18, §3.1]. They are connected by the *Etherington reciprocity law* below [26, 27],<sup>8</sup>

$$d_L = (1 + z) d_G. \quad (5)$$

Therefore, the expressions above must be rewritten to become applicable for  $z \gtrsim 0.2$  as follows,

$$d_{\text{obs}} = d_i, \quad (6)$$

$$V_{\text{obs}} = V_i = \frac{4}{3}\pi(d_i)^3, \quad (7)$$

$$N_{\text{obs}} = N_i = B_i (d_i)^{D_i}, \quad (8)$$

$$\gamma_{\text{obs}}^* = \gamma_i^* = \frac{N_i}{V_i} = \frac{3B_i}{4\pi}(d_i)^{D_i-3}, \quad (9)$$

where  $i = (L, G)$  according to the chosen distance definition. Both the constant  $B_i$  and the fractal dimension  $D_i$  are now dependent on a specific distance measure because  $N_i$  is counted considering the limits given by each cosmological distance. So, for a given  $z$  each  $d_i$  will produce its respective  $V_i$ ,  $N_i$ ,  $B_i$  and  $D_i$ .

Regarding the actual implementation of the above methodology with real data coming from galaxy redshift surveys, two remarks are noteworthy. First,  $N_{\text{obs}}$  is viewed here as a radial average, that is, galaxies are counted at larger and larger radius. There are, of course, other ways of obtaining this quantity from the data, for instance, as a statistical average. However, the radial average method is based on the fact that this is how fractal ideas are depicted in relativistic cosmological models, where galaxies are represented as particles in a classical fluid described by state, not statistical, quantities [6, 15, 18].

The second remark concerns the existence of a decades old result coming from models of relativistic fractal cosmologies which predicts that the number density, and so the fractal dimension, will decrease for larger redshift values [15, Fig. 1], [16, Figs. 1 and 3] and [18, Fig. 2]. In these models the average number density is defined through radial averaging. Hence, the shift in  $D$  to smaller values as  $z$  increases, particularly for  $z > 1$ , is an effect to be expected observationally. In fact, such prediction was already acknowledged in previous works where the fractal dimension was derived through the radial average of cumulative number counts from observational surveys having deep galaxy redshift values [9–11]. See also [29, Figs. 3,4,9,10] and [30, Figs. 7–12].

---

<sup>8</sup>Eq. (5) is the second version of the reciprocity law [see 27, for a brief historical account of this law], whose first version contains the *observer area distance* (not used in this study). The first version of the reciprocity law is also known in the literature as the *distance duality relation* [28].

### 3. COSMOS2020 Survey

The COSMOS2020 catalog [21] is a multiwavelength dataset that combines  $izYJHK$  imaging from UltraVISTA Data Release 4 [31],  $U$ -band observations from the Canada-France-Hawaii-Telescope (CFHT) MegaCam instrument [32], ultradeep optical data from Subaru’s Hyper Suprime-Cam (HSC) [33], and a comprehensive compilation of mid-infrared imaging from Spitzer’s Infrared Array Camera (IRAC) obtained across the COSMOS field. The observed region covers approximately  $2 \text{ deg}^2$ , spanning  $1.54 \leq \text{Dec, (deg)} \leq 2.88$  and  $149.22 \leq \text{RA, (deg)} \leq 150.81$ . Each new release of the catalog incorporates deeper observations and more advanced data-processing techniques, improving the detection of faint galaxies and extending the sample to higher redshifts. For instance, the COSMOS2020 includes approximately 1.7 million galaxies, reaching depths of  $i \sim 27$ , whereas COSMOS2015 [34] contained about 500,000 galaxies down to  $K_s \lesssim 24$ .

One of the key additions in COSMOS2020 is the secondary photometric catalog known as FARMER, a profile-fitting extraction tool that delivers self-consistent photometry without requiring PSF homogenization or aperture corrections. This is an advantage when combining images with different resolutions. As shown in Ref. [21], FARMER magnitudes are consistent with those obtained using traditional SExtractor [35], but the former provides more accurate photometry for fainter galaxies.

As discussed in the previous section, our analysis relies on galaxy number counts and cosmological distance estimates, making photometric redshifts ( $\text{photo-}z$ ) a key observational parameter. These redshifts are derived through spectral energy distribution (SED) fitting, obtained with LePHARE [36] and EAZY [37], following the methodology described in Ref. [38]. In this work, we adopted the LePHARE measurements derived for the FARMER photometry.

## 4. Data Selection

In order to minimize unreliable measurements we removed objects with estimated stellar masses below  $10^7 M_\odot$ . Such very low-mass systems are a challenge for characterization in galaxy surveys and may arise from inappropriate assumptions in the adopted star-formation histories or dust extinction models [39]. In addition, we considered only galaxies with measurements in the  $NUV$ ,  $r$  and  $K$ , as these are essential for the selection to be described below. After applying these criteria our sample was reduced to 852,988 galaxies.

### 4.1. Magnitude limit

Fractal studies of galaxy distributions depend on the use of volume-limited samples. However, astronomical catalogs are typically limited by apparent magnitude, which introduces a redshift-dependent bias in the observed galaxy distribution. To mitigate this effect, we adopted an observational efficiency threshold defined by an absolute magnitude limit  $M_{\text{lim}}$  defined by

$$M_{\text{lim}} = i - 5 \cdot \log(d_L) - 25, \quad (10)$$

where  $i = 27$  is the apparent magnitude in the  $i$ -band and  $d_L$  is the luminosity distance in Mpc.

Using absolute magnitudes in the  $i$ -band derived by the LePHARE best-fit models, Fig. 1 shows the objects' redshift evolution. Galaxies with absolute magnitudes brighter than  $M_{\text{lim}}$  are marked in black and constituted our reduced subsample. A small number of objects appear at the extreme high-redshift tail of the distribution and, therefore, we imposed an additional cut at  $z = 6$ . Hence, the COSMOS2020 subsample was further reduced to 633,496 galaxies.

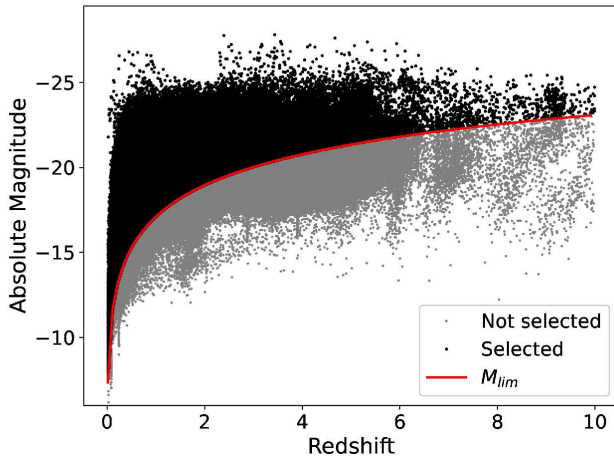


Figure 1: Absolute magnitude in the  $i$ -band as a function of redshift for the initial sample of COSMOS2020. Black circles indicate galaxies that lie above the red solid line, which represents the limiting threshold  $M_{\text{lim}}$  defined by Eq. (10), while grey circles mark those that fall below it and were discarded in this study.

#### 4.2. Color-type populations

Color-color diagrams are one of the most traditional methodologies used to separate different galaxy types such as the red sequence, blue cloud, and green valley [e.g. 40–43]. Blue galaxies are typically star-forming systems with relatively high specific star formation rates (sSFR;  $\log \text{sSFR} > -9$ ), red galaxies are quiescent with low sSFR ( $\log \text{sSFR} < -10$ ), and green valley galaxies represent transitional objects with intermediate properties. Following the classifications defined by Ref. [44, Eq. (2)], we used absolute magnitudes in the  $NUV$ ,  $r$ , and  $K$  bands to construct  $(NUV - r)$  versus  $(r - K)$  color–color diagrams and select each sample of galaxy type. In total, the sample includes 544,814 blue galaxies and 51,226 red galaxies, while 37,456 objects fall within the green-valley population. Figure 2 shows these diagrams, highlighting the three galaxy categories across six redshift intervals:  $(z \leq 1)$ ,  $(1 < z \leq 2)$ ,  $(2 < z \leq 3)$ ,  $(3 < z \leq 4)$ ,  $(4 < z \leq 5)$ , and  $(5 < z \leq 6)$ .

By examining Fig. 2 and the galaxy redshift distribution in Fig. 3, one can notice that for  $z > 4$  the number of detected objects drops sharply across all galaxy types. For this reason we further restricted our analysis and discussion to the range  $z \leq 4$ , leading to a *final subsample* containing 618,952 galaxies.

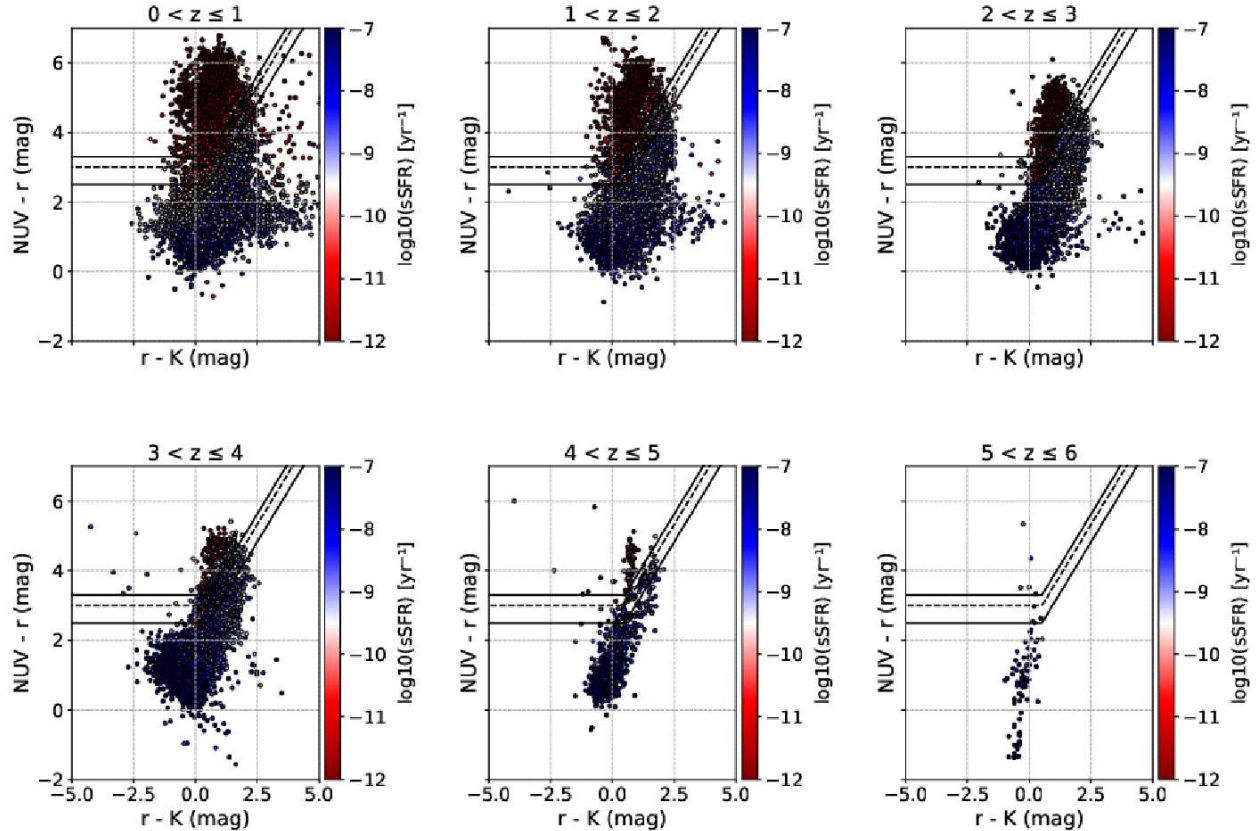


Figure 2:  $NUV - r$  vs.  $r - K$  color-color diagrams for 6 equally lengthened redshift intervals. Solid lines correspond to the criterion defined by Ref. [44, Eq. (2)], which separates galaxies into three classes: red (above the superior solid line), blue (below the inferior solid line), and green (in between the solid lines). The colorbar represents the sSFR.

## 5. Results

Analysis of the observed number density  $\gamma^*$  in terms of the distances measures  $d_L$  and  $d_G$  in log-log plots shown in Fig. 4 revealed two well-defined power-law intervals separated by the observational boundary at  $z = 1$ . The slopes obtained through linear regression were converted into fractal dimensions using the relation  $D = 3 + \text{slope}$ , resulting in different values for  $D$  according to the galaxy color type.

For *blue* galaxies we obtained  $D_L = 1.72 \pm 0.04$  and  $D_G = 1.98 \pm 0.05$  at  $z < 1$ , and  $D_L = 0.43 \pm 0.01$  and  $D_G = 0.25 \pm 0.07$  in the range  $1 < z \leq 4$ . *Red* galaxies exhibited lower initial dimensions, having  $D_L = 1.48 \pm 0.02$  and  $D_G = 1.72 \pm 0.04$  for  $z < 1$ , which drop to  $D_L = 0.28 \pm 0.01$  and  $D_G = 0.04 \pm 0.01$  for  $1 < z \leq 4$ . Finally, the *green valley* galaxies yielded  $D_L = 1.42 \pm 0.02$  and  $D_G = 1.70 \pm 0.03$  for  $z < 1$ , decreasing to  $D_L = 0.34 \pm 0.01$  and  $D_G = 0.15 \pm 0.03$  at the higher redshift interval of  $1 < z \leq 4$ . These results are collected in Tab. 1.

The consistency of this color type distinction even after accounting for photometric redshift error propagation suggests that the fractal dimension does provide an observational

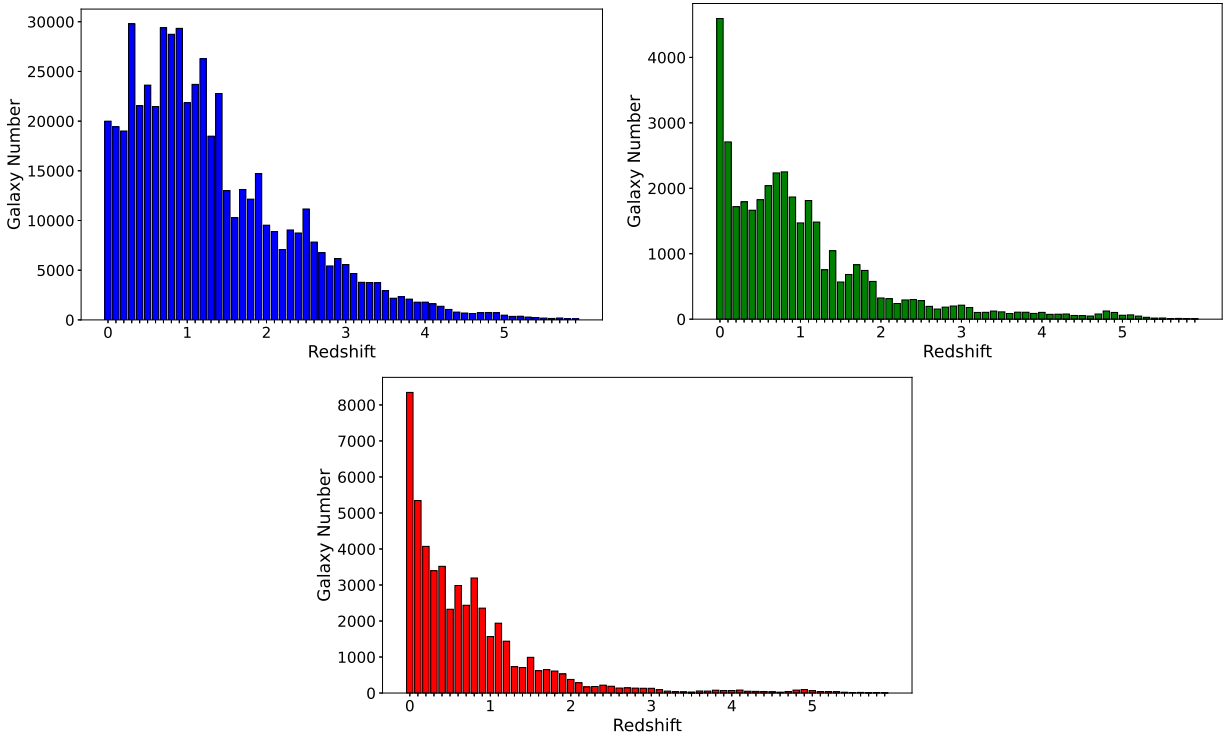


Figure 3: Histogram of the redshift distribution of blue (top left), green valley (top right) and red galaxy types (bottom). After discarding galaxies having  $z > 4$  we ended up with a final subsample containing 618,952 objects, constituted by 532,190 blue galaxies, 50,383 red ones, and 36,379 objects being classified as galaxies belonging to the green-valley.

parameter capable of distinguishing different galaxy population types in terms of color. This interpretation is reinforced by the fact that the blue population, dominated by recent star formation, consistently exhibits the highest fractal dimensions, indicating a relatively dense spatial filling. In contrast, quiescent galaxies occupy regions of lower global density, resulting in lower dimensional values. The intermediate position of green valley galaxies suggests that the decline in star formation rate is already affecting the large-scale topology, albeit less markedly than in red galaxies.

This pattern replicates with greater resolution and detail the blue-red contrast observed in previous surveys, namely COSMOS2015, SPLASH, and UltraVISTA [10, 11], which showed that each population displays a characteristic fractal dimensional “signature.” The results obtained here (see Tab. 1) present a clear gradient:  $D_{\text{blue}} > D_{\text{red}} > D_{\text{green}}$  for  $z < 1$ , and  $D_{\text{blue}} > D_{\text{green}} > D_{\text{red}}$  for  $1 < z \leq 4$ . Such ordering for blue and red color galaxy populations was previously pointed out by Ref. [11] that the fractal dimension can be used as a descriptor of an intrinsic property, remaining stable for a star-forming populations but contracting significantly in quiescent ones. Thus, the present dataset reinforces the central proposition of this work, namely that  $D$  seems to provide a descriptive indicator of color differentiation which might mean distinguishing evolutionary galaxy classes.

In addition to internal consistency, our values align with the fractal dimension ranges of

Color	$D_L (z < 1)$	$D_L (1 < z \leq 4)$	$D_G (z < 1)$	$D_G (1 < z \leq 4)$
Blue	$1.72 \pm 0.04$	$0.43 \pm 0.01$	$1.98 \pm 0.05$	$0.25 \pm 0.07$
Red	$1.48 \pm 0.02$	$0.28 \pm 0.01$	$1.72 \pm 0.04$	$0.04 \pm 0.01$
Green	$1.42 \pm 0.02$	$0.34 \pm 0.01$	$1.70 \pm 0.03$	$0.15 \pm 0.03$

Table 1: Results in two redshift scales of the COSMOS2020 galaxy survey fractal analysis in the reduced subsample shown by color. The single fractal dimensions  $D_L$  and  $D_G$  were obtained through the luminosity distance  $d_L$  and galaxy area distance  $d_G$ , also known as transverse comoving distance, respectively. The very low values  $D_L = 0.28 \pm 0.01$  and  $D_G = 0.04 \pm 0.01$  for red galaxies at the higher redshift interval of  $1 < z \leq 4$ , the lowest fractal dimension results found in this study, indicate the virtual absence of these galaxy color types in that redshift range, as shown in Fig. 3

$1.42 - 1.83$  for  $z < 1$  and  $0.23 - 0.81$  for  $1 < z \leq 6$  obtained with the UltraVISTA DR1 using similar methodologies [10], but without galaxy distinction by color. The recurrence of a “dimensional spectrum” associated with galaxy colors or star formation rates suggests that  $D$  captures physical information that complements traditional photometric indices. In particular, it quantifies the degree of spatial clustering through a single quantity that appears to remain stable under moderate changes in magnitude cuts and in the choice of cosmological distance measures.

Some limitations should be noted. The dimensions for  $z > 1$  are affected by sparse statistics, especially within the red galaxy samples, and by the propagation of photometric redshift uncertainties. Deeper spectroscopic surveys would be required to validate the persistence of these differences at earlier cosmic times. Additionally, the employed method relies on a single fractal dimension approach. Therefore, multifractal extensions could reveal internal variations in  $D$  within the same category and further enhance the method as a classification tool.

## 6. Conclusions

This work investigated the applicability of the single fractal dimension  $D$  as a parameter for distinguishing galaxy populations by color using large-scale redshift survey data. The subsample of 618,952 galaxies from the COSMOS2020 survey catalog, whose selection was based on strict photometric and completeness criteria in the  $NUV$ ,  $r$ , and  $K$  bands up to  $z = 4$ , enabled the identification of three distinct galaxy populations by color types, namely, blue, green, and red. This was done through color-color diagrams depicting star formation rates.

Cumulative number counts were assumed to be a function of cosmological distances by means of the *Pietronero-Wertz number distance relation*, which in turn allowed us to write the *de Vaucouleurs density power-law* that relates galaxy number densities to distances. The single fractal dimension  $D$  were then derived from plots constituted by the linearized slope of the power-law.

Fractal dimensions obtained this way from the above mentioned COSMOS2020 survey subsample revealed systematic variations correlated with galaxy color types. Star-forming,

or blue color galaxies, consistently presented the highest fractal dimensions, indicating a denser spatial distribution, while low star-formation, or red color galaxies, showed lower dimensions, suggesting that these galaxies are found in less dense regions. Green color galaxies showed approximate intermediary values for higher redshift values, possibly suggesting them as being a transition between active and inactive types.

The results showed two fractal dimensional gradients, namely,  $D_{\text{blue}} > D_{\text{red}} > D_{\text{green}}$  for  $z < 1$ , and  $D_{\text{blue}} > D_{\text{green}} > D_{\text{red}}$  for  $1 < z \leq 4$ , gradient which showed to be robust even when accounting for photometric redshift uncertainties. These results reinforce previous findings by Ref. [11] who showed fractal dimension dependency on galaxy color types. Despite data limitations at high redshifts, especially for the red population, and the use of single slope models, our analysis supports the use of fractal dimension as a parameter to discriminate galaxies by their colors.

In summary, the fractal geometry methodology presented here seems to offer a straightforward quantitative way to track observational aspects of large-scale galaxy populations that goes beyond the discussion if the large-scale structure of the Universe eventually turns into a homogeneous distribution, a subject that has so far constrained the application of fractal geometry in cosmological studies. Hence, fractal methods such as the one exposed here could in principle be applied to other observational galaxy features, because they provide a sensitive diagnostic for how galaxies trace the evolving cosmic web.

## Acknowledgments

S.T. acknowledges financial support from *Coordenação de Aperfeiçoamento de Pessoal de Nível Superior - Brasil* (CAPES) - Finance Code 001. A.R.L acknowledges the grant number 2025/09544-0 from *São Paulo Research Foundation* (FAPESP) and financial support from *Consejo Nacional de Investigaciones Científicas y Técnicas* (CONICET). M.B.R. received partial financial support from the *Rio de Janeiro State Research Funding Agency* (FAPERJ), grant number E-26/210.552/2024.

## Author contribution

A.E.L., J.C.S., A.C.S.T. and M.V.T. developed the Python code for data selection, reduction and analysis, and produced the first text draft. S.T. and A.R.L. supervised and contributed to the code development. A.R.L. and M.B.R. provided the theoretical underpinning, supervised the whole research and edited the final text.

## Data Availability Statement

This manuscript has no associated data.

## Code Availability Statement

This manuscript has no associated code/software.

## Conflict of interest

The authors declare that they have no known competing financial interests or personal relationships that could have appeared to influence the work reported in this paper.

## References

- [1] X.-P. Zhu, J.-M. Dai, C.-J. Bian, Y. Chen, S. Chen, C. Hu, Galaxy morphology classification with deep convolutional neural networks, *Astrophys. Space Sci.* 364 (4) (2019). arXiv:1807.10406, doi:10.1007/s10509-019-3540-1.
- [2] B. B. Mandelbrot, *The Fractal Geometry of Nature*, Freeman, New York, 1983.
- [3] L. Pietronero, The fractal structure of the universe: Correlations of galaxies and clusters and the average mass density, *Physica A* 144 (1987) 257–284. doi:10.1016/0378-4371(87)90191-9.
- [4] P. H. Coleman, L. Pietronero, The fractal structure of the Universe, *Physics Reports* 213 (6) (1992) 311–389. doi:10.1016/0370-1573(92)90112-D.
- [5] M. B. Ribeiro, A. Y. Miguelote, Fractals and the distribution of galaxies, *Brazilian J. Phys.* 28 (2) (1998) 132–160, arXiv:astro-ph/9803218. doi:10.1590/S0103-97331998000200007.
- [6] B. J. Souza, O. L. Santos-Pereira, M. B. Ribeiro, Galaxy mergers in a fractal cosmology, *Eur. Phys. J. C* 85 (2025) 455. arXiv:2504.09649, doi:10.1140/epjc/s10052-025-14191-0.
- [7] F. Sylos Labini, M. Montuori, L. Pietronero, Scale-invariance of galaxy clustering, *Physics Reports* 293 (2) (1998) 61–226. arXiv:astro-ph/9711073, doi:10.1016/S0370-1573(97)00044-6.
- [8] A. Gabrielli, F. Sylos Labini, M. Joyce, L. Pietronero, *Statistical Physics for Cosmic Structures*, Springer, Berlin, 2005.
- [9] G. Conde-Saavedra, A. Iribarrem, M. B. Ribeiro, Fractal analysis of the galaxy distribution in the redshift range  $0.45 < z < 5.0$ , *Physica A* 417 (2015) 332–344. arXiv:1409.5409, doi:10.1016/j.physa.2014.09.044.
- [10] S. Teles, A. R. Lopes, M. B. Ribeiro, Fractal analysis of the UltraVISTA galaxy survey, *Phys. Lett. B* 813 (2021) 136034. arXiv:2012.07164, doi:10.1016/j.physletb.2020.136034.
- [11] S. Teles, A. R. Lopes, M. B. Ribeiro, Galaxy distributions as fractal systems, *Eur. Phys. J. C* 82 (2022) 896. arXiv:2209.15044, doi:10.1140/epjc/s10052-022-10866-04.
- [12] S. Teles, Galaxy distribution systems as fractals, Undergraduate dissertation, Valongo Observatory, Universidade Federal do Rio de Janeiro (2023). doi:10.48550/arXiv.2310.00104.
- [13] M. I. Scrimgeour, et al., The WiggleZ Dark Energy Survey: The transition to large-scale cosmic homogeneity, *Mon. Not. R. Astron. Soc.* 425 (1) (2012) 116–134. arXiv:1205.6812v2, doi:10.1111/j.1365-2966.2012.21402.x.
- [14] R. S. Gonçalves, G. C. Carvalho, U. Andrade, C. A. Bengaly, J. C. Carvalho, J. Alcaniz, Measuring the cosmic homogeneity scale with SDSS-IV DR16 quasars, *Journal of Cosmology and Astroparticle Physics* 2021 (03) (2021) 029, arXiv:2010.06635v2. doi:10.1088/1475-7516/2021/03/029.
- [15] M. B. Ribeiro, On modeling a relativistic hierarchical (fractal) cosmology by Tolman’s space-time. II. Analysis of the Einstein-de Sitter model, *Astrophys. J.* 395 (1992) 29. arXiv:0807.0869, doi:10.1086/171628.
- [16] M. B. Ribeiro, Observations in the Einstein-de Sitter cosmology: Dust statistics and limits of apparent homogeneity, *Astrophys. J.* 441 (1995) 477. arXiv:astro-ph/9910145, doi:10.1086/175374.
- [17] M. B. Ribeiro, The apparent fractal conjecture, *Fractals* 9 (2001) 237–240. arXiv:gr-qc/9909093, doi:10.1142/S0218348X01000646.
- [18] M. B. Ribeiro, The apparent fractal conjecture: Scaling features in standard cosmologies, *Gen. Rel. Grav.* 33 (2001) 1699. arXiv:astro-ph/0104181, doi:10.1023/A:1013095316494.
- [19] M. B. Ribeiro, Cosmological distances and fractal statistics of galaxy distribution, *Astron. & Astrophys.* 429 (2005) 65–74. arXiv:astro-ph/0408316, doi:10.1051/0004-6361:20041469.

[20] L. J. Rangel Lemos, M. B. Ribeiro, Spatial and observational homogeneities of the galaxy distribution in standard cosmologies, *Astron. & Astrophys.* 488 (2008) 55. arXiv:0805.3336, doi:10.1051/0004-6361:20077978.

[21] J. R. Weaver, et al., COSMOS2020: A panchromatic view of the universe to  $z \sim 10$  from two complementary catalogs, *Astrophys. J. Supp.* 258 (1) (2022) 11. doi:10.3847/1538-4365/ac3078.

[22] J. R. Wertz, Newtonian hierarchical cosmology, Ph.D. thesis, University of Texas at Austin (1970).

[23] J. R. Wertz, A Newtonian big-bang hierarchical cosmological model, *Astrophys. J.* 164 (1971) 227. doi:10.1086/150834.

[24] M. B. Ribeiro, Relativistic fractal cosmologies, in: D. W. Hobill, A. Burd, A. Coley (Eds.), *Deterministic Chaos in General Relativity*, Vol. 332 of B, NATO ANSI, Plenum, New York, 1994, pp. 269–296. arXiv:0910.4877, doi:10.1007/978-1-4757-9993-4\_15.

[25] G. de Vaucouleurs, The case for a hierarchical cosmology: Recent observations indicate that hierarchical clustering is a basic factor in cosmology, *Science* 167 (1970) 1203–1213. doi:10.1126/science.167.3922.1203.

[26] I. M. H. Etherington, On the definition of distance in general relativity, *Phil. Mag.* 15 (7) (1933) 761, Reprinted: *Gen. Rel. Grav.*, 39(2007)1055–1067. doi:10.1007/s10714-007-0447-x.

[27] G. F. R. Ellis, On the definition of distance in General Relativity: I. M. H. Etherington (*Philosophical Magazine* ser. 7, vol. 15, 761, (1933)), *Gen. Rel. Grav.* 39 (2007) 1047–1052. doi:10.1007/s10714-006-0355-5.

[28] R. F. L. Holanda, J. A. S. Lima, M. B. Ribeiro, Testing the distance-duality relation with galaxy clusters and supernovae Ia, *Astrophys. J. Lett.* 722 (2010) L233–L237. arXiv:1005.4458, doi:10.1088/2041-8205/722/2/L233.

[29] V. V. L. Albani, A. S. Iribarrem, M. B. Ribeiro, W. R. Stoeger, Differential density statistics of the galaxy distribution and the luminosity function, *Astrophys. J.* 657 (2007) 760. arXiv:astro-ph/0611032, doi:10.1086/510520.

[30] A. S. Iribarrem, A. R. Lopes, M. B. Ribeiro, W. R. Stoeger, Relativistic cosmology number densities and the luminosity function, *Astron. & Astrophys.* 539 (2012) A112. arXiv:1201.5571, doi:10.1051/0004-6361/201117535.

[31] A. Moneti, et al., The fourth UltraVISTA data release (DR4): II/373, <https://cdsarc.cds.unistra.fr/viz-bin/cat/II/373> (2023).

[32] M. Sawicki, et al., The CFHT large area U-band deep survey (CLAUDS), *Mon. Not. R. Astron. Soc.* (2019). arXiv:1909.05898, doi:10.1093/mnras/stz2522.

[33] H. Aihara, et al., Second data release of the Hyper Suprime-Cam Subaru strategic program, *Publ. Astron. Soc. Japan* 71 (6) (2019). arXiv:1905.12221, doi:10.1093/pasj/psz103.

[34] C. Laigle, et al., The COSMOS2015 catalog: Exploring the  $1 < z < 6$  universe with half a million galaxies, *ApJS* 224 (2) (2016) 24. doi:10.3847/0067-0049/224/2/24.

[35] E. Bertin, S. Arnouts, SExtractor: Software for source extraction., *Astron. & Astrophys. Supp.* 117 (1996) 393–404. doi:10.1051/aas:1996164.

[36] S. Arnouts, L. Moscardini, E. Vanzella, S. Colombi, S. Cristiani, A. Fontana, E. Giallongo, S. Matarrese, P. Saracco, Measuring the redshift evolution of clustering: the Hubble Deep Field South, *Mon. Not. R. Astron. Soc.* 329 (2) (2002) 355–366. arXiv:astro-ph/0109453, doi:10.1046/j.1365-8711.2002.04988.x.

[37] G. B. Brammer, P. G. van Dokkum, P. Coppi, EAZY: A fast, public photometric redshift code, *Astrophys. J.* 686 (2) (2008) 1503–1513. doi:10.1086/591786.

[38] O. Ilbert, et al., Mass assembly in quiescent and star-forming galaxies since  $z = 4$  from UltraVISTA, *Astron. Astrophys.* 556 (2013) A55. doi:10.1051/0004-6361/201321100.

[39] M. A. C. de los Reyes, et al., Stellar Mass Calibrations for Local Low-mass Galaxies, *Astrophys. J.* 989 (1) (2025) 91. arXiv:2409.03959, doi:10.3847/1538-4357/ade4c5.

[40] E. Daddi, et al., A new photometric technique for the joint selection of star-forming and passive galaxies at  $1.4 \lesssim z \lesssim 2.5$ , *Astrophys. J.* 617 (2) (2004) 746–764. arXiv:astro-ph/0409041, doi:10.1086/425569.

[41] S. Arnouts, et al., Encoding of the infrared excess in the NUVrK color diagram for star-forming galaxies, *Astron. & Astrophys.* 558 (2013) A67. arXiv:1309.0008, doi:10.1051/0004-6361/201321768.

- [42] T. Moutard, et al., The VIPERS Multi-Lambda Survey. I. UV and near-IR observations, multi-colour catalogues, and photometric redshifts, *Astron. & Astrophys.* 590 (2016) A102. arXiv:1602.05915, doi:10.1051/0004-6361/201527945.
- [43] D. Vergani, et al., The VIMOS Public Extragalactic Redshift Survey (VIPERS). AGN feedback in [NeV] emitters, *Astron. & Astrophys.* 620 (2018) A193. arXiv:1712.08168, doi:10.1051/0004-6361/201732495.
- [44] G. Noirot, et al., Across the Green Valley with HST grisms: colour evolution, crossing time-scales, and the growth of the red sequence at  $z = 1.0\text{--}1.8$ , *Mon. Not. R. Astron. Soc.* 512 (3) (2022) 3566–3588. arXiv:2203.06185, doi:10.1093/mnras/stac668.

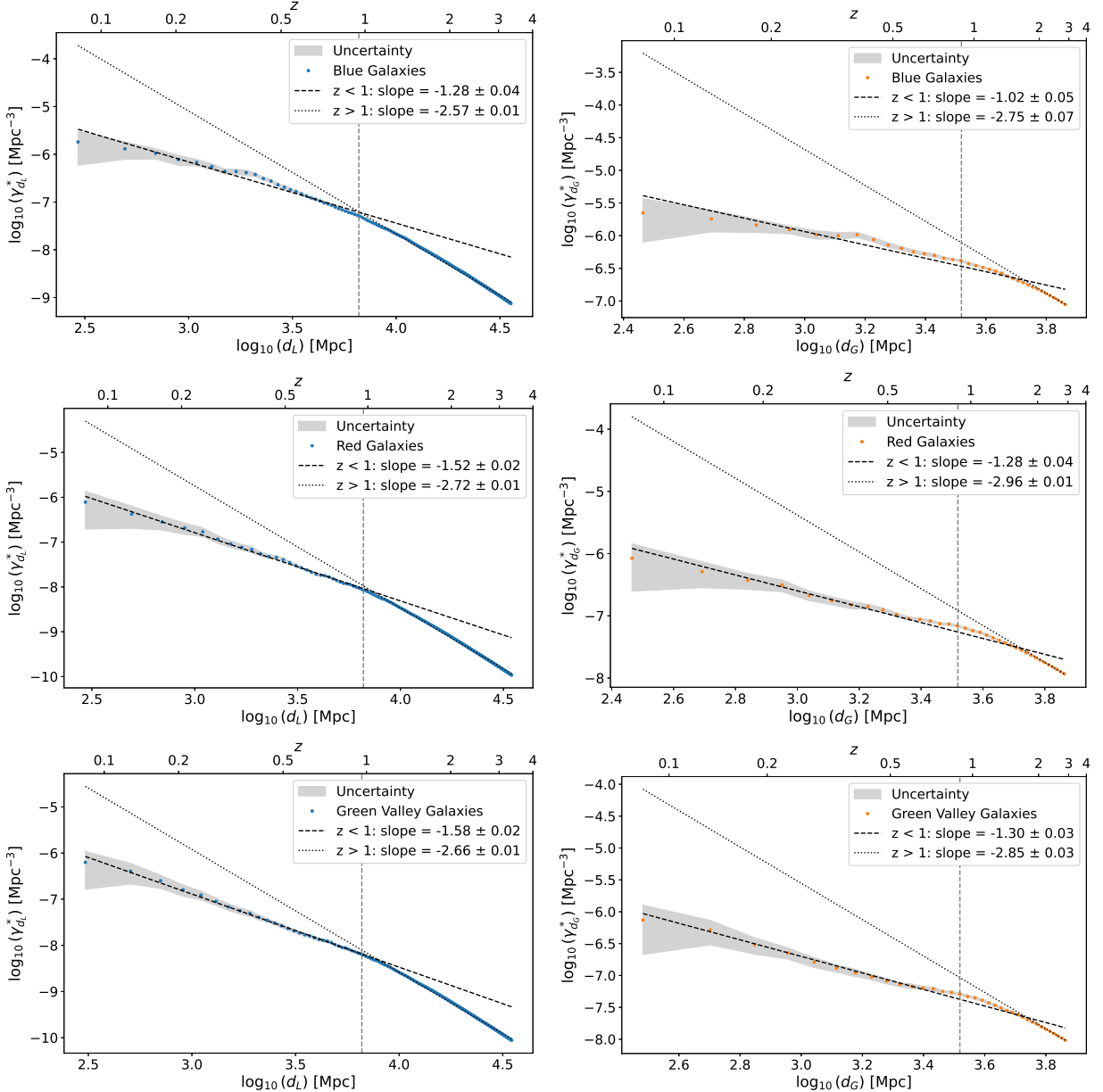


Figure 4: Galaxy number densities  $\gamma_{\text{obs}}^*$  obtained as counts per cumulative volume with steps of 200 Mpc in terms of the luminosity distance  $d_L$  and galaxy area distance  $d_G$  [19, §2] for three color type populations: blue, red and green. The shaded gray region represents the  $1\sigma$  uncertainty range derived from the upper and lower bounds of the photometric redshifts (lpzPDFU68, lpzPDFl68). The vertical dashed line marks the fractal dimension transition at  $z = 1$ .